Chapter 2

Exponential bulges in late-type spirals: A statistical approach†

In many cases the modeling of spiral galaxies by an exponential disk and an $r^{1/4}$ law bulge does not satisfactorily describe the mean radial distribution of light. This is most evident in non-linear least-square fitting techniques in which the resulting effective radius and surface brightness of the bulge are characterized by large uncertainties and are scattered over large ranges, in sharp contrast to their disk counterparts. Here we have attempted to decompose the major axis profiles of 34 late type spirals in terms of an alternative model consisting of an exponential disk and an *exponential* bulge, using seeing-convolved models. The results of this decomposition show that this model is superior in the statistical aspects of the fitting procedure, in the sense that the various goodness-of-fit indicators are better and the residuals are smaller. The fact that it also confines the parameters of the bulge to a range whose narrowness is comparable to that of the parameters of the disk, indicates that this model has the potential to give a better and more consistent description of the bulges of late type spirals.

1 Introduction

The question of decomposing the light distribution of disk galaxies into distinct components has been often addressed, and several methods and models have been proposed for this purpose (for an overview, see Simien, 1989). Most methods are based on assuming beforehand the form of the light distribution of each component and then trying to fit the sum of these forms to the observed light profiles using various fitting algorithms. The way that this general recipe is applied varies, both in terms of the exact mathematical form of the functions and in terms of the algorithm.

The use of an exponential disk to describe the outer parts of spirals is a common feature in all models (Freeman, 1970, Kormendy, 1977). The most commonly used model for the bulge is the well–known de Vaucouleurs' $r^{1/4}$ law (de Vaucouleurs, 1948) which gives a reasonably good description of the luminosity profiles of elliptical galaxies. Since the work

†Y.C. Andredakis & R.H. Sanders, Mon. Not. R. Astron. Soc. **267**, 283-296 (1994)

of de Vaucouleurs (1958) on the bulge of M31, the $r^{1/4}$ law has also been used extensively in decompositions of spirals, despite the fact that, as the photometric data increase in number and quality, significant deviations from the $r^{1/4}$ law are observed, especially in edge–on galaxies (Kormendy & Bruzual 1978, Burstein 1979, Jensen & Thuan 1979, Shaw & Gilmore 1989, Wainscoat et.al 1989). A supposed structural or evolutionary link between ellipticals and the spheroidal parts of spirals is undoubtedly a motive (most often implicit) for choosing the same fitting function, but for an objective interpretation of data such a link should not necessarily be assumed. It is necessary to try alternative fitting functions for the bulge, especially for the later types. This is supported by the great differences in colors and color gradients between these bulges and elliptical galaxies or bulges of SO's (Wirth & Shaw 1983; Balcells & Peletier 1993). Moreover, bulges often demonstrate disk–like morphology and dynamics implying that their dynamical history has been affected by the presence of the disk (Kormendy 1993 and references therein).

Alternative forms that have been considered are thick exponential disks (van der Kruit and Searle 1981, Bahcall and Kylafis 1985, Shaw and Gilmore, 1989) and exponential spheroids. There has been observational evidence in support of the exponential spheroid as a model of the light distribution of the non-thin-disk component. Star count results by Pritchet (1983) and by Gilmore and Reid (1983) for the bulge of the Galaxy point toward an exponential z–dependence. Kent et.al, (1991), using infrared photometry also show that a pure exponential law fits the inner points of the Galactic spheroid much better than the $r^{1/4}$ law.

The object of the present work is to apply the two–component decomposition scheme on a sample of 34 late-type spirals in order to compare the standard $r^{1/4}$ law for the bulge with the alternative exponential form. We show that both in terms of the standard means of evaluating the quality of the fits and in terms of the physical implications of the results, the exponential form is superior to the $r^{1/4}$ form for the bulge.

The general structure of this paper is as follows: in Section 2, we give a brief description and justification of the sample of galaxies used. In Section 3 we discuss the decomposition method and the various quantities which can serve as indicators of the goodness-of-fit. In Section 4 we present the results obtained for each of the two models that we used, along with an overall statistical comparison between them. In Section 5 we assess the reliability of our algorithm by extracting the known parameters of synthetic photometric data. This also leads to interesting conclusions on the ability of such methods to distinguish between models. In Section 6 we examine and compare the characteristic best fit parameters of the disks and the bulges derived by our proposed models. We also investigate various possible correlations between disk and spheroid parameters and compare again to similar results obtained by others. Section 7 contains a summary and discussion of our results.

2 Sample

The sample chosen is a set of 34 Sb and Sc spirals with r band photometry by Kent (1986). These are field galaxies with distances ranging from 5.6 to 165 Mpc, but mostly between 20 and 70 Mpc ($H_0 = 50$, adopted throughout). The only criterion for their selection

was that their optical rotation curves had been measured by Rubin et al. (1985). This is the principal reason we chose this medium size sample and not one of the larger available sets containing 100 galaxies or more. The kinematical data can be used later to estimate mass-to-light ratios of the various components and to calculate the distribution of dark and visible matter within the galaxies. A second motivation for choosing this particular sample is the homogeneity of the data: they were obtained at a single telescope, with the same CCD, and were reduced in the same way. In any case, this is one of the largest sets containing only Sb and Sc spirals.

The observations were originally made in the F bandpass and then reduced to the r band of the Thuan & Gunn (1976) *uvgr* system. The photometry was not deep; for most cases, it did not reach beyond 25 r mag/arcsec^2 (about 26 Bmag/arcsec^2).

The surface brightness profiles of the galaxies were obtained by fitting ellipses to the isophotes of the image (Kent 1986). For galaxies without prominent extra features (such as bars, warps etc) this method gives a profile which is equivalent to a simple cut along the axes, but with a much higher signal-to-noise ratio due to the number of points involved. The mean surface brightness along the ellipse is then plotted against its major and its minor axis lengths. Kent claims that the main source of errors is the uncertainty of the background determination along with imperfect flat-fielding of the images. He estimates that at a level of 23.5 mag/arcsec^2 errors of 0.1 mag are possible and overall they should not be larger than 0.2 mag at $\mu_r = 24$. Below, we see how various error distributions affect the decomposition results.

3 Fitting method and goodness-of-fit indicators

The algorithm applied here is the straightforward non-linear fitting of both components simultaneously to the observed light profile with respect to the parameters of the disk and the bulge; i.e., the central and effective intensities and the characteristic lengths (4 parameters in total). An important aspect of the non - linear minimization algorithms is their sensitivity to the initial values provided; in some cases "strange" initial guesses are needed to bring the searching algorithm close enough to the global minimum in the four-parameter space. For this reason, it was sometimes necessary to iterate on the initial set by searching through a small grid.

3.1 Reduced chi-square and Goodness-of-fit

Here we use two statistical measures, the reduced χ^2 and the Goodness-of-Fit, in order to assess the accuracy and overall success of a fit. The numerical value of the reduced χ^2 as a criterion for the accuracy of decompositions was first introduced by Schombert & Bothun (1987). Correlating the accuracy with which the input parameters were retrieved with the corresponding values of the reduced χ^2, they set a "credibility limit" of 2.0. Above this limit, the decomposition proved to be unreliable, at least for the error distribution they assumed. Because of the sensitivity to errors we will here avoid the use of such "credibility limits" in discussing our results.

An better indication of the fit quality can be obtained by the use of the Goodness-of-Fit, defined as:

$$Q = \int_{\chi^2}^{\infty} P_x(x^2)dx^2 \tag{1}$$

where

$$P_x(x^2) = \frac{(x^2)^{1/2(\nu-2)}e^{-x^2/2}}{2^{\nu/2},\,(\nu/2)} \tag{2}$$

is the probability distribution function for ν degrees of freedom. Q expresses the probability that a completely random set of data should have a χ^2 greater than the one found, and hence should be as close to 1 as possible. The existence of this case-independent standard and the fact that Q is an extremely rapidly decreasing function of χ^2, make it a very useful quantity for comparing theoretical models, giving a clearer image than the χ^2 test. In general, a fit should be considered acceptable for values of Q greater than 0.001 (Press et al., 1990), but it should be kept in mind that Q is also very sensitive to the errors attributed to the data. For example, a change of the order of 0.05 mag/arcsec^2 in the errors of a surface brightness profile can decrease Q by several orders of magnitude. For that reason, it should not be quoted as an *absolute* measure of whether a fit is good or not unless the errors are known to a high accuracy.

3.2 Parameter errors and fitting residuals

An important aspect of the fits to galactic profiles and of non-linear fitting procedures in general is the errors of the resulting parameters. This point has been often neglected, although the typical χ^2 minimization algorithms always give estimates for these errors in the form of the diagonal elements of the covariance matrix of the parameters. Again, these estimates depend on the uncertainties that one attributes to the data points but in more than one way: The uncertainties must be normally distributed in order to interpret the diagonal elements of the covariance matrix as real standard deviations for the parameters. While this is not always the case, the estimated errors can serve as a means of comparison between models due to the significance that they can have on any subsequent conclusions concerning the light distribution. For example, when one wants to extract mass distribution and theoretical rotation curves out of the light distribution models the errors play a particularly important role. An error of the order of 80% in the value of the bulge effective radius –something that is not unusual as is seen below– can give an uncertainty of up to 40% in the predicted rotational velocity due to the bulge in the outer parts. Ultimately, this would lead to an uncertainty of more than a factor of 2 in the derived M/L ratio.

Finally, the residuals of the fit have been used successfully in the past, to reveal systematic deviations of the profiles from the assumed models, and to allow the detection of underlying components such as thick disks, lenses, and disk-like structures (in ellipticals). Below, we will use the distribution of the residuals as an indication of whether (and how) a particular model fails to describe the actual light profiles.

4 Decomposition

When seeking a function that best describes the light distribution of the bulge, special care should be taken to account for the effects of atmospheric smearing. Especially for distant galaxies, or galaxies with small bulges, atmospheric seeing makes it impossible to resolve the innermost parts; no matter what the exact law, a steeply rising $r^{1/4}$ or a shallower alternative, the core always shows a "leveling off" that hides the underlying true distribution. The usual way to circumvent this problem is to omit the inner points from the fit (e.g. Kormendy 1977, Prieto et.al 1992). However, when we are dealing with low-resolution data, as in this case, discarding information is hardly justified. Instead, we fit the profiles using a seeing-convolved formula for the bulge (in addition, this copes with an important disadvantage of the $r^{1/4}$ law: its derivative tends to infinity as r approaches zero). Assuming that the actual two-dimensional profiles are radially symmetric and that the PSF can be adequately described by a Gaussian, the seeing-convolved profile $\Sigma_c(r)$ is given by

$$\Sigma_c(r) = \sigma^{-2} \exp(-r^2/2\sigma^2) \int_0^\infty \Sigma(x) I_0(xr/\sigma^2) \times \exp(-x^2/2\sigma^2) x dx \qquad (3)$$

where $\Sigma(r)$ is the intrinsic light distribution, σ is the dispersion of the Gaussian PSF and I_0 is the zero-order modified Bessel function of the first kind (Pritchet & Kline, 1982). The σ of the seeing Gaussian is given by Kent (1986) separately for each galaxy.

We begin by using the classical $r^{1/4}$ model for the bulge, having the form

$$\Sigma_{bulge}(r) = B_e \exp\{-7.67[(r/r_e)^{1/4} - 1]\} \qquad (4)$$

and an exponential disk:

$$\Sigma_{disk}(r) = D_0 \exp(-r/h_D). \qquad (5)$$

For the fitting, equal weights are assigned to all the points. Usually the outermost points have larger errors due to uncertainties in the determination of the sky background, lower signal-to-noise etc., and they should be assigned smaller weights. However, this makes the fit less sensitive to the possible contribution of the bulge in the regions where the disk dominates. In addition, there is no indication of the radius beyond which errors increase; therefore, we choose this simple equiweighting. Subsequent tests, assigning smaller weights to the outer points showed that the results are relatively insensitive to the weighting scheme adopted. The results of the decomposition using the above fitting functions are given in Table 1. For each galaxy, we give the values of the best-fit parameters, the uncertainties in the parameters of the bulge, the χ^2 and the goodness-of-fit (Q). In general, the fitting procedure is not very stable and for some cases a search through a grid of initial guesses is needed in order to bring the algorithm close enough to the best-fit values. For NGC 7541 no bulge parameters can be found since the presence of a dust lane causes a central dip in the profile. For NGC 701 the effective radius is fixed to 1 kpc by eye estimation; the bulge of this galaxy is too small for a free fit. For the rest of the galaxies, we can attain a full decomposition. The value of the χ^2 is calculated assuming an error of 0.1mag/arcsec^{2}for each data point.

Table 1: Results of exp. + $r^{1/4}$ decomposition

Galaxy (1)	D_0 (2)	h_D (3)	B_e (4)	ΔB_e (5)	r_e (6)	Δr_e (7)	χ^2 (8)	Q (9)
NGC701	18.98	2.92	25.12	3.05	1.00	-	1.99	1.001E-03
NGC753	20.07	6.58	23.02	.18	14.37	1.95	1.17	2.390E-01
NGC801	21.94	25.55	22.57	.11	15.59	1.50	.39	9.992E-01
NGC1085	20.05	5.31	22.76	.19	15.77	1.60	1.62	2.028E-02
NGC1087	20.26	4.64	24.19	.33	14.22	6.62	1.33	1.004E-01
NGC1325	20.34	6.15	24.12	.40	3.80	1.53	.35	9.998E-01
NGC1353	19.60	4.32	20.19	.35	.77	.18	1.01	4.510E-01
NGC1417	19.88	8.27	21.01	.49	3.25	1.19	1.92	1.780E-03
NGC1421	19.81	9.11	21.44	1.87	.66	.83	3.57	9.584E-12
NGC1620	20.06	9.65	23.05	.72	4.34	2.71	.78	8.031E-01
NGC2590	20.18	8.05	23.11	.35	14.38	5.47	1.13	2.894E-01
NGC2608	19.91	3.90	18.47	1.47	.20	.16	3.99	5.895E-12
NGC2708	19.94	3.81	22.98	.10	6.95	.78	.09	1.00E+00
NGC2715	20.35	6.13	23.61	.84	1.84	1.34	.87	6.772E-01
NGC2742	19.91	4.03	20.93	3.54	.24	.48	3.61	2.240E-11
NGC2815	22.85	14.45	23.63	.16	25.24	5.36	.68	9.137E-01
NGC2998	20.18	7.22	24.74	.23	30.98	6.83	1.07	3.629E-01
NGC3054	19.77	5.21	20.42	.65	1.01	.44	3.31	1.380E-10
NGC3067	19.05	2.38	21.43	3.83	.34	.85	2.29	9.242E-05
NGC3200	20.40	12.07	20.35	.33	1.43	.30	1.25	1.445E-01
NGC3495	20.53	4.91	23.67	2.48	.65	1.24	4.55	3.202E-18
NGC4062	19.72	2.69	22.35	1.73	.45	.55	2.33	1.083E-05
NGC4448	19.70	3.06	22.02	.52	2.83	1.41	3.83	3.472E-13
NGC4682	20.38	5.01	19.12	1.09	.09	.09	1.48	4.385E-02
NGC4800	18.79	1.21	21.45	.27	1.46	.30	1.32	1.128E-01
NGC7171	20.15	6.21	22.49	.97	1.86	1.41	1.12	3.013E-01
NGC7217	19.95	3.42	21.69	.10	5.51	.59	.31	1.00E+00
NGC7537	19.62	3.34	24.02	.39	10.85	3.47	1.59	2.466E-02
NGC7541	19.21	6.90	–	–	–	–	4.45	
NGC7606	19.66	9.01	21.25	.32	2.42	.59	1.03	4.190E-01
NGC7664	19.04	3.08	23.68	.26	12.49	1.56	1.05	3.918E-01
UGC2885	20.94	18.80	20.92	.59	2.34	.87	5.06	1.959E-21
UGC11810	20.62	7.98	23.19	.95	3.66	2.89	1.13	2.941E-01
UGC12810	20.25	12.06	16.93	4.78	.17	.37	1.20	2.209E-01

Columns in Table 1: **(1)** Object name **(2)** Central surface brightness of the disk **(3)** Disk scalelength **(4),(5)** Effective surface brightness of the bulge and its uncertainty **(6),(7)** Bulge effective radius and its uncertainty **(8)** Reduced χ^2 **(9)** Goodness of fit

The most striking feature of Table 1 is the large uncertainties in the effective surface brightness and effective radius of the bulge, especially when compared to the respective figures for the disk (not given). The uncertainty in B_e ranges from 0.1 to 4.7 mag/arcsec^2, with a mean value of $\langle \Delta B_e \rangle$ =0.87 mag/arcsec^2, while for the effective radius the corresponding range is 0.1 to 6.8 kpc, with a mean of $\langle \Delta r_e \rangle$ =1.67 kpc. These large errors can almost certainly be attributed to an intrinsic property of the $r^{1/4}$ law; i.e., it contributes a significant percentage of the total light throughout the whole profile and eventually dominates over the light of the disk at large radii. As a consequence, the results of the fitting are sensitive to the irregularities of *both* the bulge and the disk profiles (i.e. spiral arms, bars, regions of enhanced star formation, non-constant scalelengths etc.). In addition, we see in Table 1 that within a very narrow range of morphological types there are very small bulges as well as giant ones which dominate the entire profile (see Section 6).

The decomposition is repeated using an exponential rather than $r^{1/4}$ law model for the bulge; i.e.,

$$\Sigma_{bulge}(r) = 5.36 B_e \exp[-1.68(r/r_e)]. \quad (6)$$

where the effective radius and surface brightness have the same meaning as the ones for the $r^{1/4}$ law (half-total-light values). Apart from its simplicity, this fitting function falls off quickly enough to allow the disk to dominate in the outer parts and is well-behaved as r tends to zero. Its first derivative still presents a discontinuity at $r = 0$, but it is finite and no high central peak is predicted. The results of the decomposition using the exponential form for the bulge are given in Table 2. The fits prove to be very stable, the convergence to a minimum is rapid, and the use of only one initial set of parameters is sufficient for all the galaxies. These should be expected because of the simple mathematical form of the model; a better description of the data is not necessarily implied by these facts. However, when we come to examine the values of the parameters themselves and their errors, there is a striking difference compared to the $r^{1/4}$ law fits. Both bulge parameters lie in very narrow ranges that have almost no overlap with the corresponding regions of the disk parameters. The uncertainties are much smaller, decreasing by almost as much as an order of magnitude: the mean uncertainty in the effective surface brightness is 0.14 mag/arcsec^2, and the mean uncertainty of the effective radius is only 0.06 kpc. These are comparable to or even smaller than the uncertainties in the disk parameters, thus displaying the internal consistency of the model. As far as the quantitative goodness-of-fit indicators are concerned, a comparison can be easily made through the "logQ – logQ"

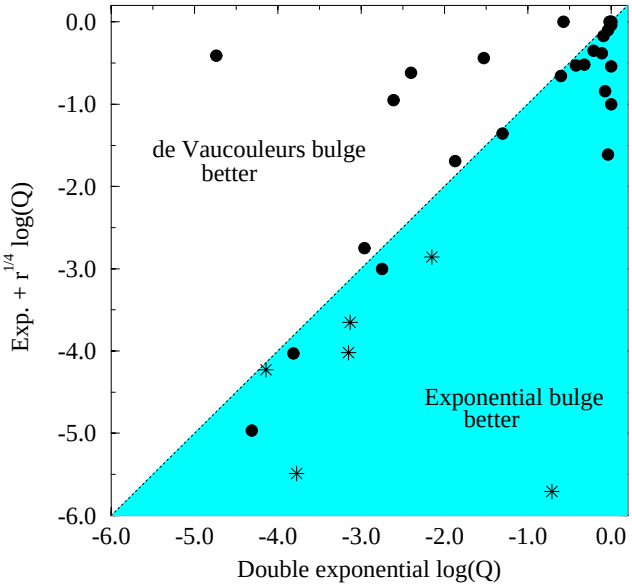

Figure 1: The "$logQ - logQ$" diagram for the 33 galaxies that could be fully decomposed. 24 points lie below the equality line, indicating a better double exponential fit. Points represented by a star ($\star$) have been shifted upwards, along lines parallel to the equality line, to make the diagram more compact and clearer.

Table 2: Results of double exponential decomposition

Galaxy (1)	D_0 (2)	h_D (3)	B_e (4)	ΔB_e (5)	r_e (6)	Δr_e (7)	χ^2 (8)	Q (9)
NGC701	19.01	2.96	22.80	.91	.99	.666	1.92	1.780E-03
NGC753	19.89	7.74	19.97	.14	2.30	.159	1.82	3.939E-03
NGC801	20.86	17.67	19.63	.09	2.74	.090	1.14	2.682E-01
NGC1085	20.46	9.36	19.63	.13	2.83	.141	1.68	1.357E-02
NGC1087	19.84	4.61	20.35	.06	.88	.035	.47	9.953E-01
NGC1325	20.23	5.86	21.23	.08	.68	.029	.33	9.999E-01
NGC1353	19.48	4.13	18.59	.11	.39	.015	.91	6.131E-01
NGC1417	19.61	7.67	18.96	.19	1.14	.076	1.98	1.088E-03
NGC1421	19.81	9.09	20.29	.29	.46	.044	3.41	7.098E-11
NGC1620	19.99	9.43	20.77	.13	1.31	.070	.67	9.178E-01
NGC2590	19.80	8.10	19.92	.07	1.93	.067	.41	9.975E-01
NGC2608	19.88	3.84	18.53	.34	.26	.019	3.97	7.317E-12
NGC2708	19.49	3.69	19.72	.06	.80	.026	.34	1.00E-00
NGC2715	20.30	5.98	21.20	.14	.51	.028	.78	8.076E-01
NGC2742	19.92	4.05	20.70	.31	.28	.024	3.51	7.350E-11
NGC2815	20.40	8.38	19.93	.05	1.73	.048	.67	9.996E-01
NGC2998	20.06	8.35	21.02	.15	2.46	.253	1.54	2.974E-02
NGC3054	19.69	5.10	19.00	.21	.58	.040	3.18	7.037E-10
NGC3067	19.05	2.38	20.50	.63	.28	.075	2.23	1.566E-04
NGC3200	20.32	11.71	19.14	.09	.95	.026	.76	8.492E-01
NGC3495	20.54	4.95	21.91	.45	.33	.083	4.27	1.708E-16
NGC4062	19.72	2.70	20.87	.36	.25	.047	2.19	4.882E-05
NGC4448	19.42	2.94	19.15	.11	.53	.029	2.05	2.951E-04
NGC4682	20.38	5.01	20.60	.17	.21	.004	1.46	4.972E-02
NGC4800	18.54	1.24	18.45	.21	.23	.020	1.88	2.456E-03
NGC7171	20.10	6.09	20.62	.18	.79	.054	.99	4.794E-01
NGC7217	19.04	3.32	18.72	.05	.81	.018	.64	9.320E-01
NGC7537	19.83	4.06	20.76	.08	1.94	.129	.66	9.134E-01
NGC7541	19.21	6.90	–	–	–	–	4.45	–
NGC7606	19.56	8.69	19.13	.09	.87	.031	.81	7.834E-01
NGC7664	22.36	9.53	20.29	.07	4.43	.182	2.48	1.809E-05
UGC2885	20.88	18.44	19.61	.19	1.51	.094	4.26	1.966E-16
UGC11810	20.53	7.77	21.02	.18	1.22	.083	1.06	3.804E-01
UGC12810	20.25	12.07	18.79	.15	.52	.008	1.17	2.506E-01

Columns in Table 2: **(1)** Object name **(2)** Central surface brightness of the disk **(3)** Disk scalelength **(4),(5)** Effective surface brightness of the bulge and its uncertainty **(6),(7)** Bulge effective radius and its uncertainty **(8)** Reduced χ^2 **(9)** Goodness of fit

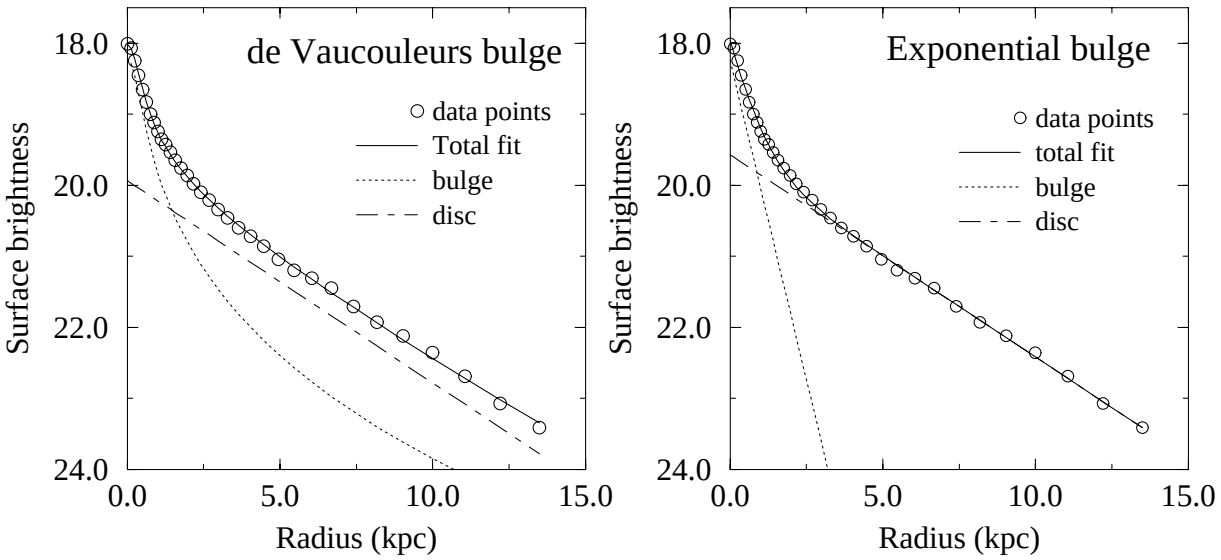

Figure 2: Decomposition of NGC2708 with both models. **(a)** *(Left panel):* $r^{1/4}$ bulge. **(b)** *(Right panel):* Exponential bulge.

diagram, given in Figure 1. It is seen that 24 points out of the 33 lie below the equality line, indicating a generally better fit by the exponential bulge. The mean value of the reduced χ^2 for these 33 galaxies is reduced from 2.02 to 1.91. This reduction in the mean value of χ^2 is by no means impressive, but this small difference can be attributed to the fact that the $r^{1/4}$ law can give in many cases a good description of a distribution that is intrinsically exponential (Section 5).

In Figures 2a and 2b we show the decomposition results for the galaxy that gives the best fit for the $r^{1/4}$ law, NGC 2708 (the fits for all the galaxies are shown in Appendix A). The $r^{1/4}$ law (Figure 2a), gives an essentially perfect fit of the inner parts, accounting for almost all the light there. The contributions of the two components become equal at about 1.5 kpc, and beyond the disk dominates. It is obvious, however, that the contribution of the $r^{1/4}$ bulge suppresses that of the disk throughout the profile. As a result, the line of the disk profile lies about 0.4 mag lower than the apparent exponential part of the actual distribution due to the non-vanishing bulge. This behavior is common also in the galaxies decomposed by Boroson (1981) and by Prieto et.al (1992). In the double exponential decomposition (Figure 2b) the situation is clearly different. The characteristic $r^{1/4}$ curvature of the intermediate zone is successfully reproduced by the superposition of the two exponential components; the bulge then falls off rapidly and allows the disk to account for all the light in the outer regions. On the average, with the exponential model the mean value of the central surface brightness of the disk is increased by about 0.15 mag/arcsec^{2}using this scheme, while the scatter is reduced from 0.80 to 0.65 mag/arcsec^2.

Why, then, does the exponential scheme give a better fit for most of the galaxies? It has been argued (Boroson, 1981, Prieto et.al, 1992) that all the departures from the $r^{1/4}$ fits are caused by enhanced star formation in regions close to the edge of the bulge. In this way, "Freeman Type II" profiles are observed, with an excessive luminosity in the

intermediate parts that cannot be accounted for by the $r^{1/4}$ model. To investigate this, we examined the fits to the profiles after subtracting the contribution of the best-fit disk *for each model*. This technique was first used by de Vaucouleurs (1958), and it is very useful in revealing any systematic deviations in the bulge profiles. The disk-subtracted inner parts of the profiles are shown in the lower panels of the plots in Appendix A, for the 32 fully decomposed galaxies. Each graph shows the nonnegative residuals of the subtraction out to a radius where the distribution still appears to be systematic, together with the corresponding best-fit models for the bulge. It is clear that the $r^{1/4}$ law generally predicts too much light in the transition region (i.e. between the bulge and disk dominated region); instead of a deficiency, we observe an *excess* of more than half a magnitude for more than half of the galaxies. This is more prominent in galaxies with small bulges, like NGC 1353, NGC 1620, NGC 3054, NGC 7171 and UGC 2885. Indeed, for these galaxies, the residuals from the disk subtraction are better described by an exponential law, regardless of the bulge law used in the fitting! On the other hand, one can identify seven spiral galaxies in which the overall bulge profile is better described by the $r^{1/4}$ law; i.e., the exponential model predicts too little light in the transition region. These are NGC 753, NGC 801, NGC 1085, NGC 1417, NGC 2998, NGC 4800, and NGC 7217. In Tables 1 and 2 we see that these galaxies are those very objects with higher Goodness-of-Fit values for the $r^{1/4}$ law bulge model (above the equality line in Fig. 1). It is clear that the relative values of Q (or χ^2) are identifying this systematic deviation of either of the two models from the true light distribution in the bulge-disk transition region. It is also clear that the exponential model provides a better description of this systematic aspect of the light distribution for most of the galaxies in this sample (25 out of 32).

5 Reliability of the decomposition results

In order to investigate the reliability of the decomposition procedure and of its results, we perform some simulations analogous to those of Schombert & Bothun (1987).

First, we examine the ability of the algorithm to recover the original parameters of artificial profiles that have been seeing-convolved and distorted with random noise. We do this using $r^{1/4}$ -law profiles, in order to determine whether the large values that we find for the effective radius are artifacts of the noise in the data or of the seeing effects. For these simulations, we use a grid of about 200 exp. disk + $r^{1/4}$ bulge models. The values of the disk parameters are kept fixed to D_0 =20.0 mag/arcsec^{2}and h_D = 4.0 kpc. The effective surface brightness of the bulge ranges from 18.0 to 23.0 mag/arcsec^{2}and the effective radius from 0.3 to 3 kpc, both in equally spaced intervals. We do not extend the range of r_e further, as we expect that small bulges are the ones more likely to give spurious results; the results justify this intuitive assumption. The artificial profiles are then convolved with a Gaussian seeing with a σ of 0.3 kpc, and Gaussian noise is added, with an r.m.s. of 0.04 mag/arcsec^2.

Applying the algorithm to these data, we find that in general the recoverability of the input parameters is excellent and that the confidence limits are ample. Only the combination of very small effective radii ($R_e \leq 1.5\sigma$) and relatively faint effective surface brightnesses

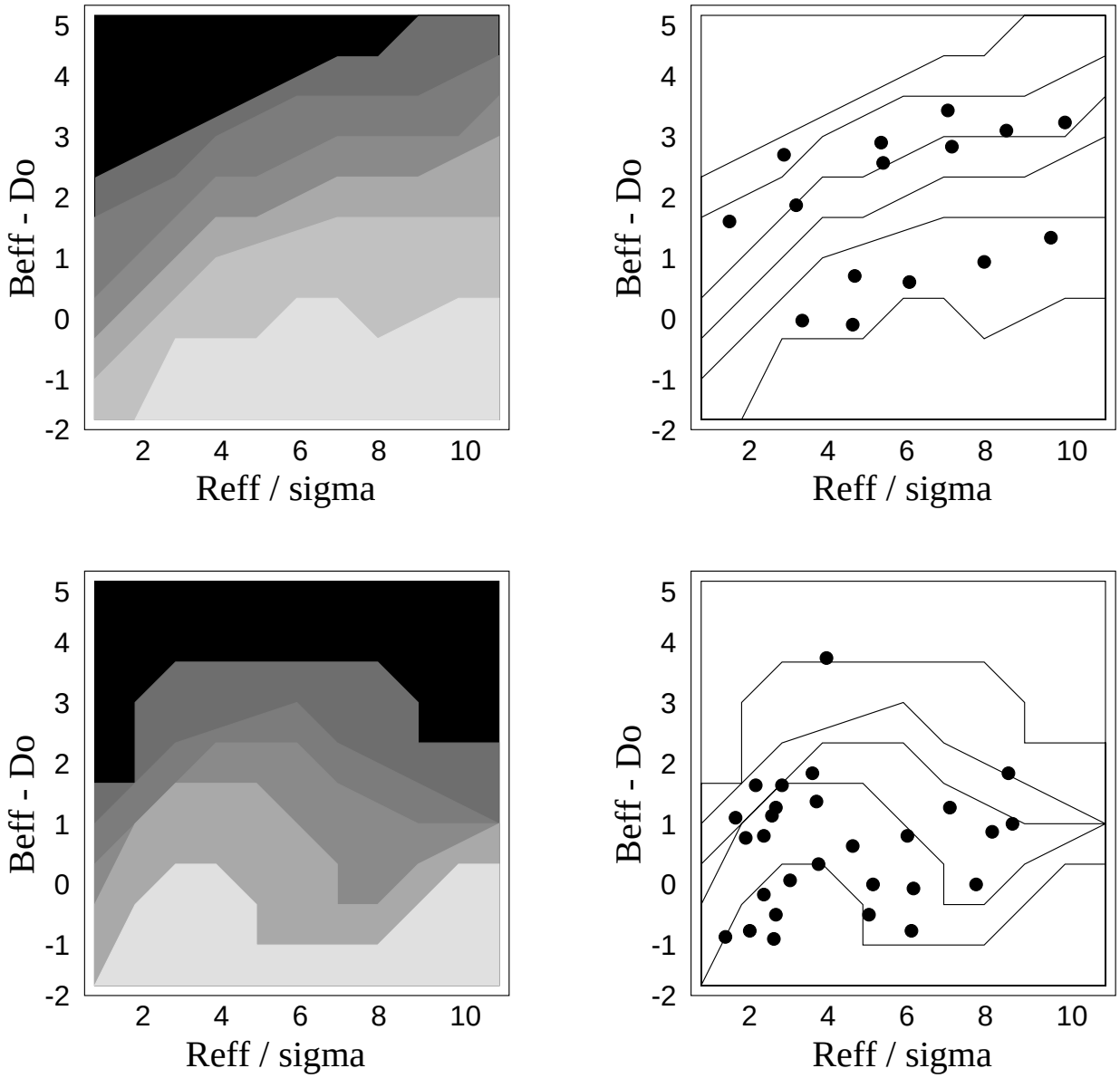

Figure 3: The "response" of the decomposition algorithms on artificial data, as a function of the prominence of the bulge (reflected by the difference $B_{eff} - D_0$) and of the effective radius relative to the seeing. (**a**) Results (in terms of the ratio of the χ^2's) of decomposing artificial [$r^{1/4}$ + exp.] data using the exponential model for the bulge. Darker regions denote increasingly comparable χ^2's of the two models. The greylevels correspond to $\chi^2_{exp}/\chi^2_{dV} = 100$, (light grey), 25, 8, 6, 4, 2, and 1 (black). (**b**) Same as (a), with the addition of the positions of the sample galaxies. (**c**) Results of decomposing artificial double exponential data using an 'model for the bulge. The contour levels are the same as in (a). (**d**) Same as (c), including the positions of the sample galaxies.

($B_e - D_0 \geq 4$) can give unreliable results. In all the other cases, the retrieval accuracy of the parameters is better than 80% for the effective radius and 0.1 mag/arcsec^{2}for the

effective surface brightness.

Secondly, we examine whether an exponential model can successfully fit a profile that intrinsically follows an $r^{1/4}$ law, and vice versa. This could happen either due to the mathematical properties of the $r^{1/4}$ law or as a result of seeing and noise effects, and would make most of the previous results meaningless.

In the first set of experiments we fit the previously mentioned grid of $r^{1/4}$ law models using an exponential bulge and an $r^{1/4}$ bulge. As a measure of the success of the fit we use the ratio of the χ^2 's given by the two models. The results are given in Figure 3a in the form of contours of this ratio as a function of the effective radius and of the relative prominence of the bulge. The black level corresponds to $\chi^2_{exp}/\chi^2_{dV} = 1$ (i.e., non-reliability region). It is seen that the exponential model can be equally well fitted to a bulge that intrinsically follows an $r^{1/4}$ law (black region) *only* if the effective radius of the latter is small in terms of the seeing radius (σ), and the effective surface brightness is more than two magnitudes fainter than the central surface brightness of the disk. Otherwise, the chi-squares given by the two models are clearly distinguishable. In Figure 3b we plot the positions of the galaxies of our sample (as determined by the results of the $r^{1/4}$ law decomposition) on this contour plot that is kept unshaded for clarity. Only 15 out of the 34 galaxies fall within the limits of the plot; the objects outside the plot lie deeper in the "reliability region". It is obvious that none of the galaxies is in the "dangerous" region, and only three lie in the region with $1 \leq \chi^2_{exp}/\chi^2_{dV} \leq 2$. The remainder, if they were really described by an $r^{1/4}$ law, would have χ^2_{dV} of one order of magnitude smaller than χ^2_{exp}.

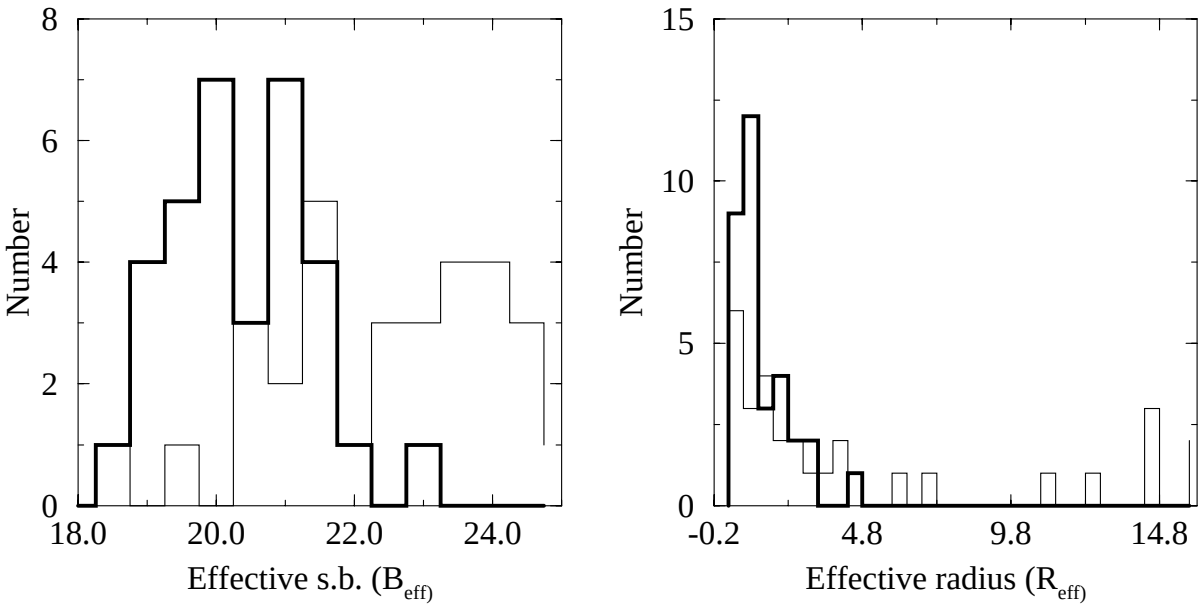

Figure 4: *Left panel:* The distribution of the effective surface brightness of the bulge. The exponential model (heavy line) gives clearly a smoother and narrower distribution than the 'model (normal line). *Right panel:* The distribution of the effective radius of the bulge. Exponential model (heavy line) and 'model (normal line).

Now we repeat this procedure using artificial double exponential models; i.e. we attempt to fit double exponential data with $r^{1/4}$ + exponential models. The results are given in

similar form in Figure 3c. We see that the regions of equal χ^2 (black regions) cover a greater fraction of the grid. This indicates that profiles that are intrinsically double exponential are better described by an $r^{1/4}$ + exponential model than vice versa. In Figure 3d we plot again the positions of the galaxies according to the results of the double exponential decomposition. In this case all of them lie within the limits set, and roughly half of the points lie quite close to the "non-reliability" region. Keeping in mind that these profiles are distorted only by Gaussian random noise and do not have the systematic large deviations from the models evidenced by actual galactic profiles, this goes far in explaining the fact that the χ^2's of the double exponential model for our galaxies are only slightly better than the ones of the $r^{1/4}$ law. In other words, it may well be that on a realistic profile the $r^{1/4}$ law mimics very well an underlying exponential distribution in the inner parts of the galaxy. If the actual light distribution in bulges were more similar to the $r^{1/4}$ law, then the exponential model would give much worse fits in terms of χ^2. The fact that the mean χ^2's are so similar for $r^{1/4}$ and exponential models is the expected result if the light distribution is approximately double exponential.

6 Distribution of the bulge properties

In most of the relevant studies (e.g. Kodaira et.al 1986 (KWO), Kent 1985, Boroson 1981, Kormendy 1977, Simien & de Vaucouleurs (1986)) the major common point as far as bulges are concerned is the very wide range covered by the values of the parameters compared to the disk. The effective surface brightness is usually found to span an interval of not less than 8 magnitudes, ranging from 18 to 26 or even 28 mag/arcsec^2. The effective radius has a minimum at about 0.4 kpc, but its maximum value is almost unconstrained, extending up to 20 kpc or more. This large scatter has given rise to questions regarding its credibility, but, since the model fit seemed satisfactory in statistical aspects, it was considered as realistic. As a consequence it is often accepted that in a single morphological type, the scatter in the parameters of one of the components (the bulge) is one order of magnitude larger than the scatter in the other one (the disk). On the other hand, normal elliptical galaxies, (i.e. excluding dwarf ellipticals) described by the same $r^{1/4}$ law, present significantly less scatter than the spheroids of spirals. It is also curious that the range in the total magnitudes of the bulges is about the same as that for the disks and not so large as might be expected from random combinations of the parameters within their ranges (KWO).

This large scatter–and its effects on luminosity ratios and other possible tracers of the Hubble sequence–has been attributed to vague "decomposition errors" (Simien, 1989). A closer look, however, shows quite clearly that: 1. The large ranges do not depend on the specific decomposition algorithm used; they are present, whether it is non-linear least squares, iterative fit or grid search. 2. They cannot be attributed to a mistreatment of the disk, since the exponential law holds extremely well in most galaxies (the possibility of a central "hole" has been investigated by Kormendy 1977). Bearing these points in mind, we would be justified to assume that the "errors" most probably lie in the very form of the model used to describe the bulge.

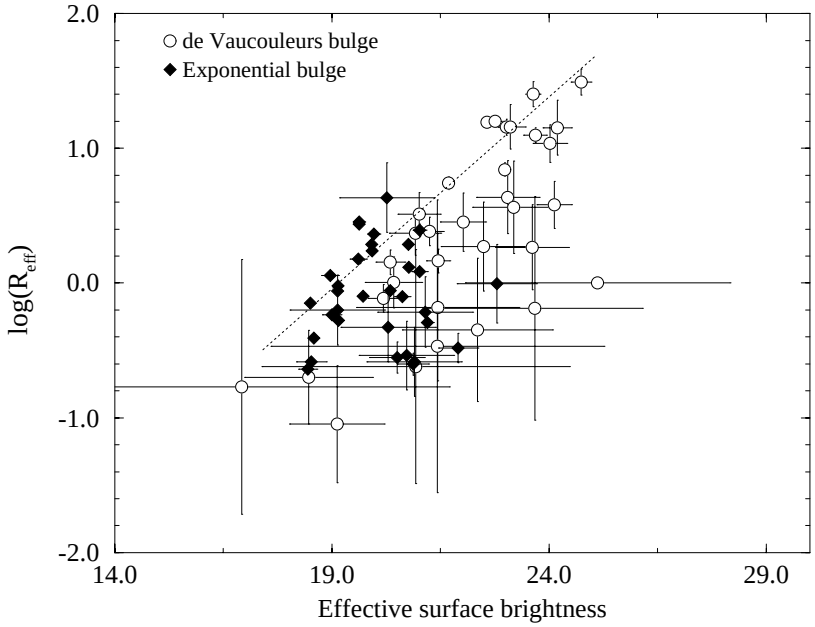

Figure 5: Bulge effective surface brightness (B_{eff}) plotted versus $logR_{eff}$. The error bars in $logR_{eff}$ have been forced to symmetry, to avoid confusion. In this and all the subsequent figures, the exponential model is represented by the filled diamonds, and the $r^{1/4}$ model by the blank ones. The "good-fit" line (dotted) is a visual guide to show that small bulges are better fit by the exponential model, while large ones by a de Vaucouleurs law.

The results presented here for the $r^{1/4}$ spheroids are fully consistent with the previous results regarding the wide distribution of the resulting parameters. The effective surface brightness ranges from 17 to 25 mag/arcsec^2, while the effective radius ranges from 0.20 to 30 kpc. The mean value of μ_e is 22.17 mag, and the standard deviation is 1.84 mag. The respective figures for the effective radius are $r_e = 6.05$ kpc, with a dispersion of 7.7 kpc.

With the exponential model for the bulge, the results are quite different. The effective surface brightnesses lie in an interval narrower by 4 magnitudes, ranging from 18.5 to 22.5 mag/arcsec^2. It is interesting to note that the standard deviation of the effective surface brightness (0.98 mag/arcsec^2) approaches that of the central surface brightness of the disk (0.60 mag/arcsec^2), pointing toward the possible existence of an analogous "Freeman's Law" for bulges. As far as the effective radius is concerned, the interval is very narrow, ranging from 0.2 to 4.5 kpc. The standard deviation is 1.05 kpc, almost one order of magnitude smaller than that of the $r^{1/4}$ model and much smaller than that of the disk scalelength ($\sim$ 4 kpc).

In Figure 4 we give the distribution of the effective surface brightnesses for the two models, in histogram form. Apart from the smaller range, the exponential model presents a distribution much closer to normal, with a peak at about 20.5 mag. The analogous histogram for the scalelengths is shown in the second panel of Figure 4. Again, the compactness of the exponential model is striking. It is also obvious that the exponential model

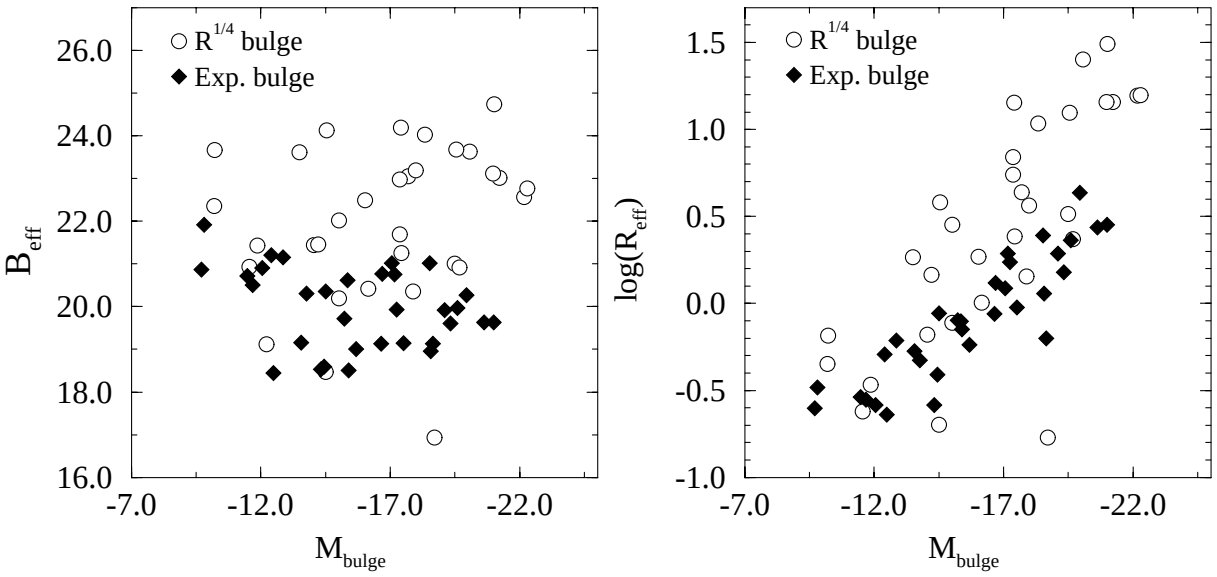

Figure 6: The effective surface brightness of the bulge (*left panel*) and the effective radius (*right panel*) plotted as a function of the absolute magnitude of the bulge. The smaller spread presented by the exponential model is obvious in both plots.

combines both smaller scalelengths and fainter effective surface brightnesses resulting in smaller total luminosities for the bulge. As a result, the range spanned by the absolute bulge magnitudes is slightly shifted toward the faint end and at the same time narrowed by about 1.5 mag.

Both of these histograms have been combined in the B_e – $\log r_e$ diagram, shown in Figure 5. This diagram has been used previously to demonstrate the general structural tendencies of spheroids. (see Fig. 3 of KWO). The points are given with their error bars in both coordinates in order to show the great differences in this respect. The difference in the total surface occupied by the points of each model is also quite obvious, showing the compactness of the exponential model. In general, fainter central magnitudes tend to be combined with larger r_e, as one would expect for a relatively narrow total luminosity range.

The relation of the central surface brightness and the scalelength to the absolute magnitude of the bulge, can be seen in Figure 6 for both models. The exponential model shows much tighter dependencies in both parameters, confirming our previous remark about the total magnitude of the spheroid.

Following the results of the above analysis, several conclusions that have been drawn in the past can be brought into question. The extremely large and faint spheroids found in previous decompositions are not real; they are most probably created by the form of the model used to describe them. Finally, as some were prompted to introduce a "standard disk" for spirals by the narrow ranges of its parameters, we would perhaps be justified to introduce the "standard bulge" –at least for late types– given the almost equally narrow ranges that the bulges demonstrate via the exponential model. These suggestions, of course, should be considered within the confidence limits set by the size of the sample and

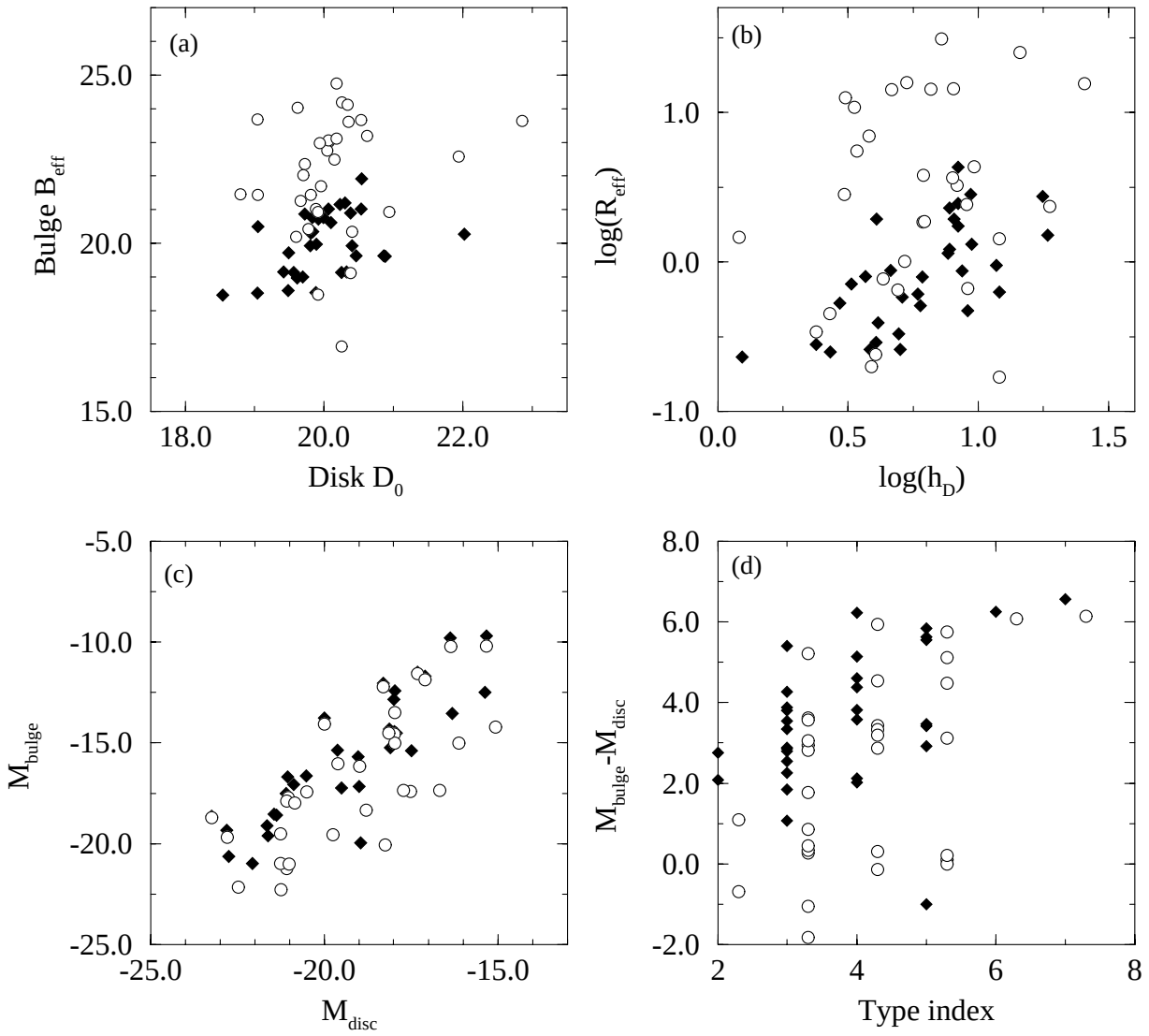

Figure 7: The interplay between the parameters of the bulge and the disk, as treated by the two models. (**a**) Effective surface brightness of the bulge *vs* central surface brightness of the disk. (**b**) Effective radius of the bulge *vs* scalelength of the disk. (**c**) Absolute magnitudes of the two components. (**d**) The bulge-to-disk ratio as a function of the type index. For all plots: *Diamonds:* Exponential bulge. *Empty circles:* de Vaucouleurs bulge.

the number of points used for the decomposition. Homogeneous data on a much larger number of disk galaxies of all types are needed in order to clarify this issue.

6.1 Bulge-disk correlations and luminosity ratios

Figure 7a shows the effective surface brightness of the bulge *vs* the central surface brightness of the disk and 7b the bulge effective radius versus the disk scalelength respectively.

Different symbols have been used for each of the two models for the bulge. It is evident that there is not any apparent correlation between B_0 and M_0, in agreement with KWO. The only additional remark is that due to the smaller range of the central bulge magnitude for the exponential model, the corresponding distribution tends to be less elongated along the M_0 axis. With respect to the scalelengths, for the $r^{1/4}$ model the points seem to be more or less randomly distributed, as in the previous studies. However, for the exponential model, there is a clear correlation of the two scalelengths in the form of a linear function in $\log - \log$ representation. The best-fit line is $\log r_e = 0.908\ \log h_D - 0.908$, with a correlation coefficient of 0.73. This suggests a linear relation between h_B and h_D.

The absolute magnitudes of the two components are plotted against each other in Figure 7c. For both models, it is clear that brighter disks are combined linearly with brighter bulges. The best-fit line is:

$$M_B = 0.57\, M_D - 9.81.$$

The correlation is quite tight, with a coefficient of 0.88 for both models.

Figure 7d shows the bulge-to-disk ratio as the absolute magnitude difference, versus the morphological type of each galaxy taken from the RC3 catalogue (de Vaucouleurs et.al, 1991). A possible correlation is more evident for the exponential model with a general tendency for the bulge to be fainter for later types. Unfortunately, both the scatter in each morphological type ($\sigma_T \geq 0.7\, mag$) and the overlap between different types are large enough to prohibit any attempt of interpretation of the Hubble sequence in this sense.

7 Conclusions

We have reconsidered the decomposition into bulge and disk components of a sample of 34 late type spirals, by using an exponential model for the bulge. The fitting was done on elliptically averaged major axis profiles of the galaxies. The principle conclusions from this procedure can be summarized as follows:

1. In order to judge the quality of a fit, multiple indicative quantities should be used. The reduced chi-square is still the most powerful indicator available, but others, such as the Goodness-of-Fit, the uncertainties of the parameters and the distribution of the residuals are also useful in discriminating between alternative models.

2. The $r^{1/4}$ law, despite the fact that it describes satisfactorily the profiles of elliptical galaxies, proved to be rather inadequate for the description of the bulges of late-type spirals. Its special mathematical (infinite derivatives, weak dependence on the length parameter) and physical (contribution at large radii) characteristics have given rise to awkward results about the characteristic properties of bulges. Using this model, the effective surface brightnesses spanned a range of about 10 magnitudes, while the respective range for the effective radii is 20 kpc. This is in sharp contrast to the ranges of the parameters of the disks, which are much smaller. Using a simple exponential law for the surface brightness of the bulge, these ranges are decreased dramatically (4 magnitudes and 4 kpc respectively), and we derive a much more consistent picture of the relevant sizes and the correlations that might exist between these two components. At the same time, the exponential model

is superior in every statistical aspect of the fitting procedure, giving a lower χ^2 for most of the galaxies, and much smaller uncertainties for the parameters.

We do not wish to claim here that the exponential light distribution provides a perfect description of all spiral bulges. The low Q - values for many of the fits and a visual inspection of the fitting residuals (Appendix A) demonstrate that this is certainly not the case. Moreover, the range of morphological types considered here is quite small; it may well be that the $r^{1/4}$ law is superior in early-type spirals, as implied for example by the "good-fit' line in Fig. 5 (if so, this in itself may indicate a different formation and dynamical history for bulges of late versus early types). But this work does suggest that the mathematical advantages of the exponential form, as reflected by the relative ease in achieving fits, may well be providing a more accurate picture of the relevant size scales, surface brightnesses, and total luminosities of bulges; that the large scatter found in these parameters in previous studies is an artifact of the fitting function used. It should also be stressed that the use of an inappropriate fitting function for the bulge can give misleading results on disk parameters; the significant contribution of the $r^{1/4}$ law at large radii erroneously decreases the derived disk surface brightness. In addition, the placement of the spiral bulges on a fundamental plane coincident with or analogous to that of ellipticals, can be significantly facilitated by a model that gives small scatter in the parameters. It may well be that the offsets found in the recent attempts to do this (Dressler 1987, Bender et.al 1992) have been caused by errors in the bulge-disk decomposition using the $r^{1/4}$ law.

References

Bahcall J.N., Kylafis N.D., 1985 ApJ, 288, 252
Balcells M., Peletier R.F., AJ, 1994, 107, 135
Bender R., Burstein D., Faber S.M., 1992, ApJ, 399, 462
Bevington P.R., 1969, *Data reduction and error analysis for the Physical Sciences,* eds. Mc Graw Hill
Boroson T., 1981 ApJSS, 46, 177
Burstein D., 1979, ApJ, 234, 829
de Vaucouleurs G., 1948, Ann. d'Ap., 11, 247
de Vaucouleurs G., 1958, ApJ, 128, 465
de Vaucouleurs G., de Vaucouleurs A., Corwin H. G., Buta R. J.,
Paturel G., Fouque P., 1991, *Third Reference Catalogue of Bright Galaxies* (New York: Springer Verlag)
Dressler A., 1987, ApJ, 317, 1
Freeman K., 1970, ApJ, 160, 811
Gilmore G., Reid N., 1983, MNRAS, 202, 1022
Jensen E.B., Thuan T.X., 1979, in *Photometry, Kinematics and Dynamics of Galaxies* (Austin: University of Texas Press)
Kent S.M., 1983, ApJ, 266, 562
Kent S.M., 1985, ApJSS, 59, 115
Kent S.M., 1986, AJ, 91, 1301
Kent S.M., Dame T., Fazio G., 1991, ApJ, 378, 131
Kodaira K., Masaaki W., Okamura S., 1986 ApJSS, 62, 703
Kormendy J., 1977, ApJ, 217, 406

Kormendy J., Bruzual A., 1978, ApJ, 223, L63
Kormendy J., 1993, in *Galactic Bulges*, IAU Symp. 153, (Kluwer, Dordrecht)
Press W.H., Teukolsky S.A., Flannery B.P., Vetterling W.T., 1986, *Numerical Recipes,* eds. Cambridge University Press
Prieto M., Beckman J.E., Cepa J., Varela A.M., 1992, A&A, 257, 85
Pritchet C., Kline M.I., 1981, AJ, 86, 1859
Rubin V.C. Burstein D., Ford W.K., Thonnard N., 1985, ApJ, 289, 81
Schombert J.M., Bothun G.D., 1987 AJ, 93, 60
Shaw M.A., Gilmore G., 1989 MNRAS, 237, 903
Simien F., de Vaucouleurs G., 1986, ApJ, 302, 564
Simien F., 1988 in *The World of Galaxies*, (New York: Springer Verlag)
Thuan T.X., Gunn J.E., 1976, PASP, 88, 543
van der Kruit P.C., Searle L., 1981, A&A, 95, 105
Wainscoat R.J., Freeman K.C., Hyland A.R., 1989, ApJ, 337, 163

A Plots of exponential fits and residuals

Here we give the double exponential fits to the profiles along with the residuals of the subtraction of the disk. The fits are shifted upwards by approximately 2.5 magnitudes for clarity; the blank circles represent the observed profile, the dashed and dot-dash lines stand for the bulge and the disk components, and the thicker solid line stands for the total predicted profile (bulge + disk). The bulge profile is shown only out to the point where $\mu_{bulge} - \mu_{disk} < 2$, to avoid confusion with the second plot.

As far as the residuals are concerned (lower plots) the filled circles are the result of the subtraction of the disk given by the double exponential model, and the dashed line is the bulge of the same model. The blank circles and the dotted line are the corresponding residuals and bulge of the [exp. $+ r^{1/4}$] model. The plots extend out to the point where the residuals do not seem to follow any systematic distributions any more and are dominated by irregularities in the disk.

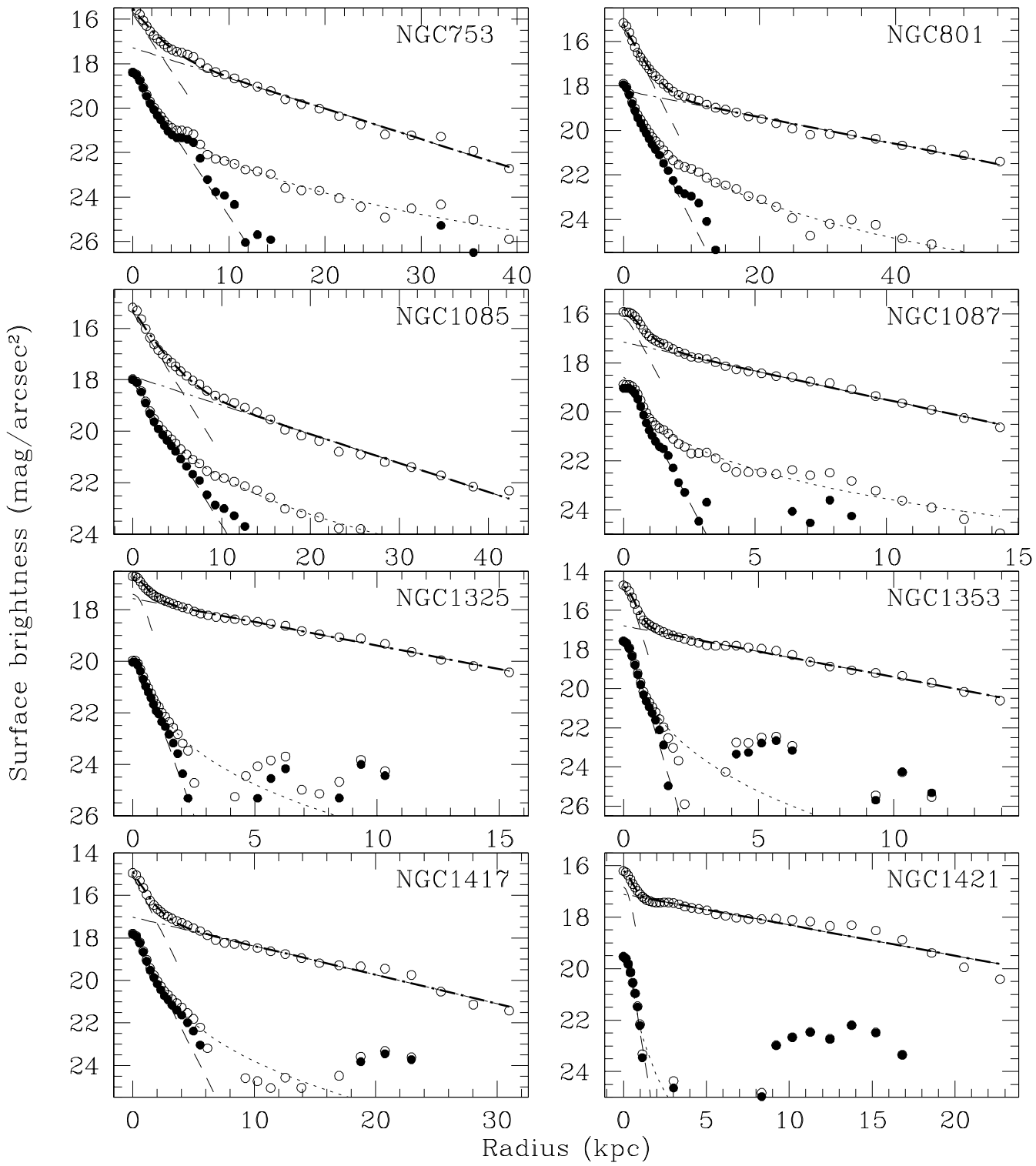

Figure 1: Double exponential fits to the total surface brightness (*upper plot in each panel*) and residuals from the disk subtraction, for both bulge models. (*lower plot*).

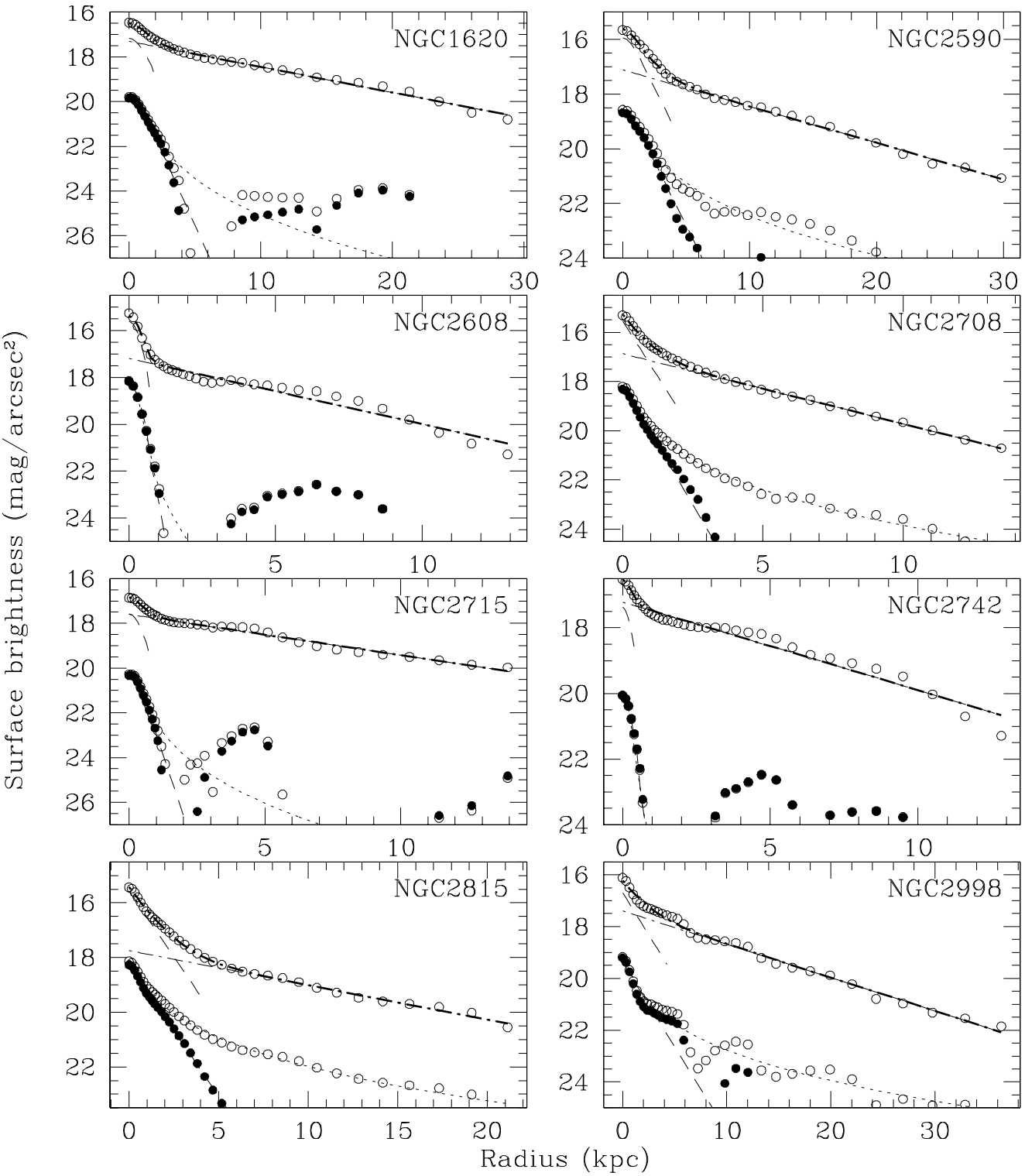

Figure 1: Continued

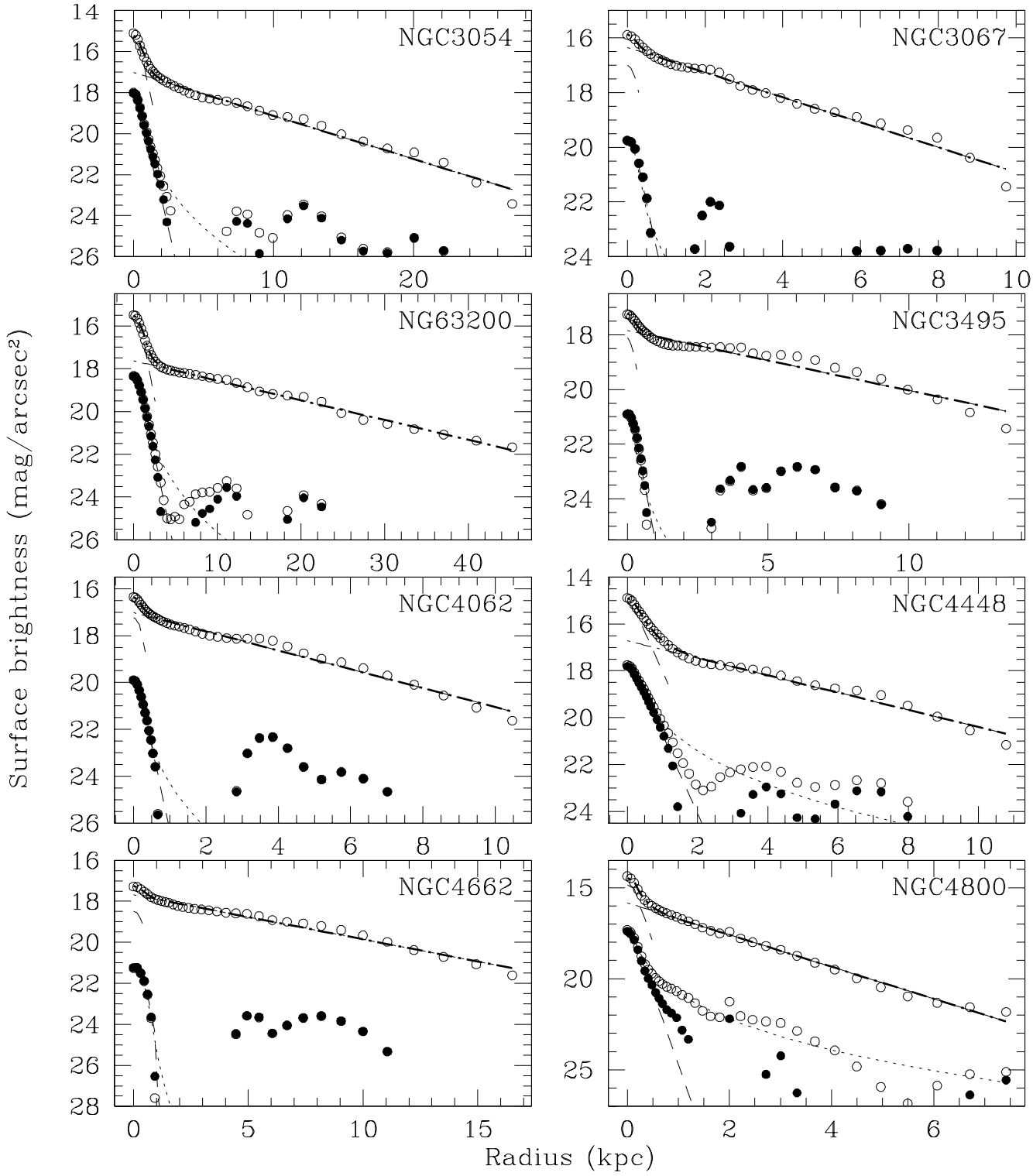

Figure 1: Continued

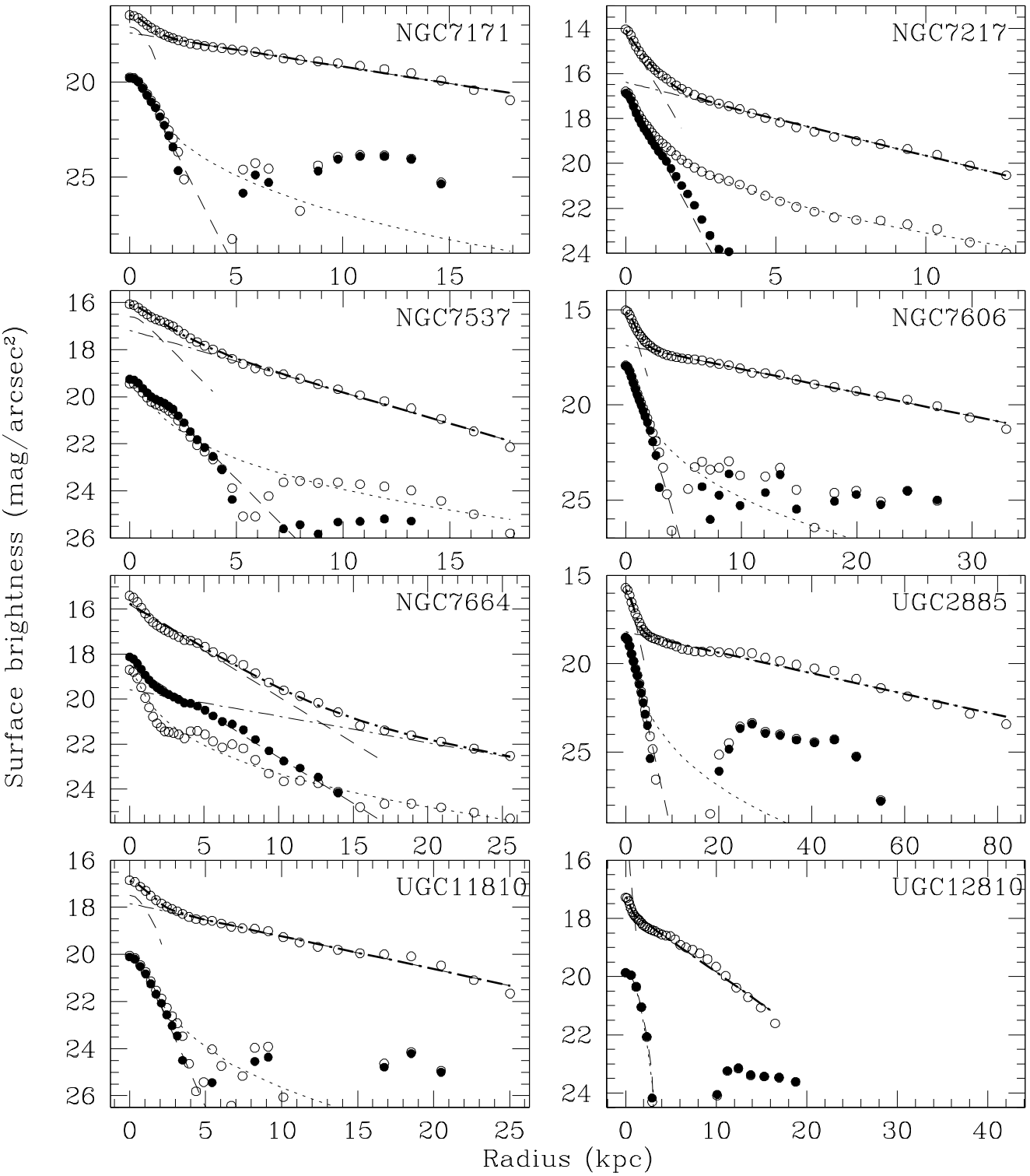

Figure 1: Continued